DEMOSAICING BASED ON WAVELET ANALYSIS OF THE LUMINANCE COMPONENT

Daniele Menon and Giancarlo Calvagno

Department of Information Engineering, University of Padova
via Gradenigo 6b - 35131 Padova, Italy
{menond, calvagno}@dei.unipd.it

ABSTRACT

Most color digital cameras apply a color filter array to capture the scene, requiring an interpolation of the subsampled color components to obtain the full resolution image. Therefore, if reconstruction is not performed correctly, noticeable artifacts are produced, which result more evident in the detailed parts of the image. In this paper we propose a demosaicing algorithm based on directional filtering that uses a novel approach to locate the details of the image. To this purpose, edge-estimation is performed on the luminance component of the image in order to give a more reliable information, and the properties of the wavelet transform are used to estimate the edge directions. Experimental results proved the effectiveness of this approach, giving high performance in PSNR, and good estimates of image details too.

Index Terms— Image reconstruction, interpolation, image edge analysis, wavelet transforms.

1. INTRODUCTION

A digital color image is composed of three primary color values at each pixel location. However, most digital cameras capture the scene with a single-sensor technology based on a Color Filter Array (CFA), where only one color value is measured at each spatial location. The two missing color values have to be reconstructed and this estimation process is known as *demosaicing*. The most common CFA is the pattern proposed by Bayer in [1], where downsampled versions of red, green, and blue planes are arranged as shown in Fig. 1(a).

In literature, many approaches have been proposed to estimate the full-color image, and a good review of them is given in [2]. Usually, the inter-channel correlation existing between the three color planes is used to estimate the missing values. In [3, 4] the high-frequencies of each color component are refined on the basis of the high-frequencies of the other colors. Moreover, many algorithms perform the interpolation exploiting the edge-direction information provided by the sensor data, in order to avoid artifacts near the borders of the objects. Some algorithms apply an edge-detection operator to decide the direction of the interpolation [5] or carry out a weighted sum of horizontal and vertical interpolations [6]. Other approaches compute two estimates of the image through horizontal and vertical interpolation, respectively, then the best reconstruction is chosen [7, 8, 9] or a fusion of both of them is calculated [10]. Instead, in [11, 12] the properties of the spectrum of the CFA image are discusses and, using suitable filters, the luminance of the image is reconstructed, from which an estimate of the full-color image is obtained. In this paper, a new approach to demosaicing is proposed, exploiting a wavelet-based analysis of the luminance component to drive an adaptive interpolation algorithm of the color components of the image.

2. WAVELET-BASED EDGE-INFORMATION EXTRACTION

Many image demosaicing approaches follow an adaptive strategy to extract information from the given data to fill in the unknown pixels values. Adaptive interpolation allows to exploit the local behavior of the image in order to adapt the reconstruction to the discontinuities and irregularities peculiar to natural images. However, in an adaptive approach image analysis plays a fundamental role since an erroneous estimation can introduce several artifacts, especially near the edges or boundaries between regions.

Information about image singularities can be gained in a wavelet framework, exploiting the wavelet property of extracting the horizontal and vertical details of an image [13].

Let $\theta(x)$ be a *smoothing function* (i.e., a function whose integral is equal to 1 and that converges to 0 at infinity). We assume that $\theta(x)$ is differentiable and define

$$\psi(x) = \frac{d\theta(x)}{dx}. \tag{1}$$

The integral of $\psi(x)$ is equal to zero, $\int_{-\infty}^{+\infty} \psi(x)dx = 0$, hence $\psi(x)$ can be considered a wavelet. We denote with $\psi_s(x)$ the dilation by a scaling factor s of $\psi(x)$,

$$\psi_s(x) = \frac{1}{s}\psi\left(\frac{x}{s}\right), \tag{2}$$

and with $\theta_s(x)$ the dilation of $\theta(x)$. The wavelet transform of

a function $f(x)$ at scale s and position x is computed by

$$W_s f(x) = f * \psi_s(x). \tag{3}$$

From the linearity of convolution and derivation, we have

$$W_s f(x) = f * s\frac{d\theta_s}{dx}(x) = s\frac{d}{dx}\left(f * \theta_s\right)(x). \tag{4}$$

Therefore, the wavelet transform $W_s f(x)$ is equivalent to the first derivative of the signal smoothed at the scale s. So, the extrema of the absolute value of the wavelet transform correspond to the inflection point of $f * \theta_s$ and, in particular, the maxima of $|W_s f(x)|$ are in correspondence of the sharp variation points of $f * \theta_s$. Moreover, the larger is the value of the maxima, the sharper is the transition of the signal. It is proved in [13] that this result can be extended to the discrete wavelet transform.

Therefore, analysis with the wavelet transform can locate discontinuities and variations in a signal. This is valid also for an image, which is a bidimensional signal $f(x, y)$, where the wavelet transform can be applied by defining two wavelet functions $\psi^H(x, y)$ and $\psi^V(x, y)$ such that

$$\psi^H(x, y) = \frac{\partial\theta(x, y)}{\partial x}, \qquad \psi^V(x, y) = \frac{\partial\theta(x, y)}{\partial y}. \tag{5}$$

Similarly to (4), applying $\psi^H(x, y)$ and $\psi^V(x, y)$ over $f(x, y)$ we obtain:

$$\begin{aligned} W_s^H f(x, y) &= s\frac{\partial}{\partial x}\left(f * \theta_s\right)(x, y) \\ W_s^V f(x, y) &= s\frac{\partial}{\partial y}\left(f * \theta_s\right)(x, y), \end{aligned} \tag{6}$$

hence edge points can be located from the local extrema of $W_s^H f(x, y)$ and $W_s^V f(x, y)$. Moreover, comparing these two components we can estimate the direction of the edges. In fact, given a region I_0 of the image, larger absolute values of $W_s^H f(x, y)$ with respect to the absolute values of $W_s^V f(x, y)$, with $(x, y) \in I_0$, indicate sharper variations along the horizontal direction in the signal domain, and vice versa.

It should be observed that wavelet extrema detection cannot be used for the magnification of a subsampled image, unless an extrapolation process of the missing details is performed [14]. However, if it is possible to obtain an estimation, even imprecise, of the image details, wavelet-based analysis can be used to detect edges and adaptively interpolate the subsampled image.

In this paper, we propose to perform the estimation of the details on the luminance component of the image, and to use this information to adaptively demosaic the CFA image. In the next section, we describe the approach followed to obtain the luminance from the Bayer-sampled values.

3. LUMINANCE ESTIMATION

Let $I(x, y) = [R_0(x, y),\ G_0(x, y),\ B_0(x, y)]$ the original color image representing the scene. Then, the CFA image is

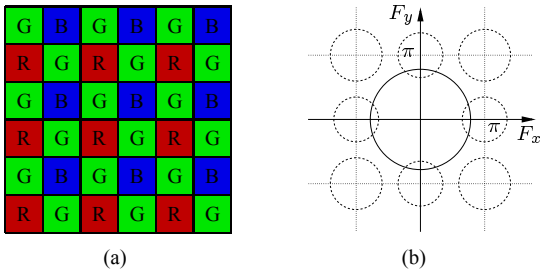

Fig. 1. (a) Bayer pattern and (b) support of the spectrum of a CFA image: luminance component (solid circle) and chrominance components (dotted circles).

given by $I_{CFA}(x, y) = R_S(x, y) + G_S(x, y) + B_S(x, y)$, where R_S, G_S and B_S are the subsampled color components acquired by the sensor. Their relationship with the original color components can be expressed as follows [11]:

$$\begin{aligned} R_S(x, y) &= \tfrac{1}{4}R_0(x, y)(1 - \cos\pi x)(1 + \cos\pi y) \\ G_S(x, y) &= \tfrac{1}{2}G_0(x, y)(1 + \cos\pi x \cos\pi y) \\ B_S(x, y) &= \tfrac{1}{4}B_0(x, y)(1 + \cos\pi x)(1 - \cos\pi y). \end{aligned} \tag{7}$$

Then, considering the terms in (7), I_{CFA} can be expressed as

$$\begin{aligned} I_{CFA}(x, y) &= \tfrac{1}{4}[R_0(x, y) + 2G_0(x, y) + B_0(x, y)] \\ &\quad + \tfrac{1}{4}[B_0(x, y) - R_0(x, y)](\cos\pi x - \cos\pi y) \\ &+ \tfrac{1}{4}[-R_0(x, y) + 2G_0(x, y) - B_0(x, y)]\cos\pi x \cos\pi y. \end{aligned} \tag{8}$$

Therefore, the CFA image has a luminance component given by $\frac{1}{4}[R_0(x, y) + 2G_0(x, y) + B_0(x, y)]$ and two modulated color difference components (chrominances). From its spectrum support (see Fig. 1(b)) it is possible to identify nine regions containing the energy of the image, where the central region corresponds to the luminance and the others to the modulated chrominance values. Since these components are not necessarily band-limited, aliasing is possible and this leads to various artifacts in the reconstructed images. The design of a low-pass filter to separate the luminance from the chrominances is not trivial and affects the interpolation performances, especially for detailed images, as reported in [11].

However in [12] it is observed that in the quincunx-placed green pixels the color difference term given by $\frac{1}{4}[B_0(x, y) - R_0(x, y)](\cos\pi x - \cos\pi y)$ vanishes. Therefore, in correspondence to these locations, the spectrum of the CFA image does not present the four chrominance components modulated at $(0, \pm\pi)$ and $(\pm\pi, 0)$, respectively, and this simplifies the design of the low-pass filter. In [12] Lian *et al.* propose a 5×5 filter that gives good performance for the estimation of the luminance in the green pixels. However, the same filter cannot be applied in the red and blue pixels.

Therefore, we use the filter proposed by Lian *et al.* in the green pixels, while for the red and blue locations we design a low-pass filter H_c that eliminates the aliasing due to all

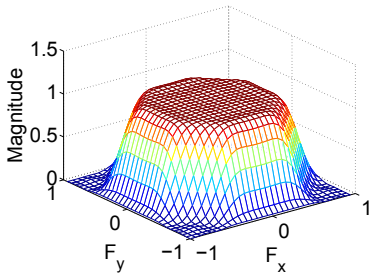

Fig. 2. Frequency response of the filter H_c.

the modulated chrominance components. The filter H_c has a 11×11 support and it is designed using the window method, imposing circular symmetry and a normalized passband frequency of 0.85 (see Fig. 2).

4. PROPOSED ALGORITHM

4.1. Color reconstruction

The proposed color reconstruction approach try to accurately estimate even the finest details exploiting the properties of the wavelets described in Section 2. The first step computes an estimation of the luminance according to the approach described in Section 3 to have a full-resolution image that is used to detect edges and image discontinuities. Then, the reconstructed luminance $\hat{L}(x,y)$ is decomposed with an analysis filter bank that performs an undecimated wavelet transform. The two components $\hat{L}_{LH}(x,y)$ and $\hat{L}_{HL}(x,y)$ are obtained as in Fig. 3, where H_0 and H_1 denote low-pass and high-pass filters, respectively. As reported in Section 2, the absolute values of $\hat{L}_{LH}(x,y)$ are large in correspondence of vertical details, and the same holds for $\hat{L}_{HL}(x,y)$ and the horizontal details. Then, by comparing these two components, we can make some hypothesis on the edge directions. Therefore, we calculate the energies of $\hat{L}_{LH}(x,y)$ and $\hat{L}_{HL}(x,y)$, denoting them with $e_{LH}(x,y)$ and $e_{HL}(x,y)$, respectively, and use them to compute two classifiers of the edge-direction at each pixel:

$$\begin{aligned} w_h(x,y) &= \frac{F * e_{HL}(x,y)}{F * e_{HL}(x,y) + F * e_{LH}(x,y)} \\ w_v(x,y) &= \frac{F * e_{LH}(x,y)}{F * e_{HL}(x,y) + F * e_{LH}(x,y)}, \end{aligned} \quad (9)$$

where F is a spatial averaging kernel. Initially F has size 3×3, however if $w_h(x,y) \simeq w_v(x,y)$, the size of the kernel is increased, in order to more effectively discriminate regions where horizontal and vertical details have the same energy from the regions where false high-frequencies are been created by an incorrect estimation of $\hat{L}$.

The two classifiers w_h and w_v are used to adaptively interpolate the green component by estimating the missing green samples as

$$\hat{G}(x,y) = w_h(x,y)\hat{G}_h(x,y) + w_v(x,y)\hat{G}_v(x,y) \quad (10)$$

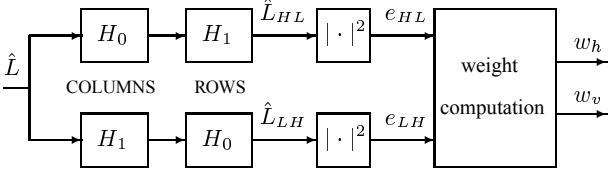

Fig. 3. Block diagram of the procedure for calculating the directional classifiers using the wavelet transform.

where $\hat{G}_h(x,y)$ and $\hat{G}_v(x,y)$ are the horizontal and vertical interpolations of the green plane obtained with the filters described in [9].

After the estimation of the green channel, the red and blue components are reconstructed through the interpolation of the color differences. As a first step, the red and blue channels are filled in the green locations through bilinear interpolation of $R - \hat{G}$ and $B - \hat{G}$ respectively, and then the red samples in the blue locations are estimated as

$$\begin{aligned} \hat{R}(x,y) &= B(x,y) \\ &+ \frac{w_h(x,y)}{2}\Big(\hat{D}_{RB}(x-1,y) + \hat{D}_{RB}(x+1,y)\Big) \\ &+ \frac{w_v(x,y)}{2}\Big(\hat{D}_{RB}(x,y-1) + \hat{D}_{RB}(x,y+1)\Big) \end{aligned} \quad (11)$$

where $\hat{D}_{RB}(x,y) = \hat{R}(x,y) - \hat{B}(x,y)$. The same strategy is applied for the reconstruction of the blue component in the red locations.

4.2. Image Enhancements

Once the full-color image is reconstructed, some techniques can be applied to enhance the final quality. In fact, it is known that color differences of original natural images present most of the energy at low frequencies, while the reconstructed images have a large amount of energy also in the mid frequencies of the color differences. A first approach to improve the reconstruction consists in filtering the differences between the color channels with the filter $[0.5\ 0\ 0.5]$, both horizontally and vertically, using the two weights w_h and w_v to adapt the refinement to the local behavior of the image. Then the refined color differences are used to correct the estimated color values. A second approach is that of applying a median filter to the color differences, as in [8].

5. RESULTS

To evaluate the performance of the proposed method, we compare its experimental results with those obtained by other recent demosaicing techniques. In this comparison, the biorthogonal wavelets of Cohen, Daubechies and Feauveau are used, however similar results are obtained with other wavelet bases. Both the two enhancement techniques explained in Section 4.2 are tested. We denote with PROP1 the proposed method followed by correction of color differences, and with PROP2 the proposed method followed by median filtering.

Fig. 4. Portion of the image no. 6 of the Kodak set: (a) original image; (b) image reconstructed by technique [10]; (c) image reconstructed by technique [12]; (d) image reconstructed by the proposed approach.

Method	[3]	[9]	[10]	[12]	PROP1	PROP2
1	38.16	37.00	38.52	37.80	38.67	**39.13**
2	39.10	40.70	**41.23**	40.91	38.50	39.43
3	37.48	37.65	38.38	**38.43**	38.13	38.37
4	39.01	39.43	40.32	38.40	40.28	**40.64**
5	41.48	41.88	42.41	**43.08**	41.86	42.23
6	35.89	35.58	36.21	35.66	36.70	**36.97**
7	41.92	42.54	43.03	43.00	43.03	**43.23**
8	41.33	42.38	42.08	**43.05**	42.84	42.76
9	39.59	39.43	40.31	39.69	39.96	**40.41**
10	42.16	43.20	43.17	43.12	43.61	**43.72**
11	34.72	33.41	34.85	34.08	34.75	**35.54**
12	39.02	39.55	39.93	**40.17**	39.25	39.56
13	42.13	43.17	43.46	41.56	44.05	**44.33**
14	41.17	40.91	41.61	41.82	41.52	**41.95**
15	36.70	36.24	36.61	36.99	36.68	**37.20**
16	40.03	39.93	40.62	40.24	41.03	**41.21**
17	37.82	40.19	38.13	41.03	40.69	**41.22**
18	38.97	38.08	39.14	38.97	39.18	**39.77**
19	37.93	37.93	38.81	**38.90**	38.48	38.40
20	34.49	34.51	**35.24**	35.03	34.81	35.09
Ave.	38.96	39.19	39.70	39.60	39.70	**40.06**

Table 1. PSNR for different demosaicing methods (dB).

The test images belong to the Kodak database, used also in [2]. Table 1 reports the resulting PSNR for the algorithms presented in [3, 9, 10, 12] (using the MATLAB source code provided by the authors) and for the proposed approach. The reported values are the averages of the PSNR for each color component, defined as

$$\text{PSNR} = 10 \log_{10} \frac{255^2}{\text{MSE}}. \qquad (12)$$

We can see that the proposed technique outperforms the other techniques in the majority of the cases and also the PSNR average value is the highest. Fig. 4 shows a sample of image no. 6 as interpolated with different methods. It can be noticed that the proposed approach accurately reconstructs also the finest details.

6. REFERENCES

[1] B. E. Bayer, "Color imaging array," U.S. Patent 3 971 065, July, 1976.

[2] B. K. Gunturk, J. Glotzbach, Y. Altunbasak, R. W. Schafer, and R. M. Mersereau, "Demosaicking: color filter array interpolation," *IEEE Signal Proc. Mag.*, vol. 22, pp. 44–54, Jan. 2005.

[3] B. K. Gunturk, Y. Altunbasak, and R. M. Mersereau, "Color plane interpolation using alternating projections," *IEEE Trans. Image Proc.*, vol. 11, no. 9, pp. 997–1013, Sept. 2002.

[4] X. Li, "Demosaicing by successive approximation," *IEEE Trans. Image Proc.*, vol. 14, no. 3, pp. 370–379, Mar. 2005.

[5] J. F. Hamilton and J. Adams, "Adaptive color plane interpolation in single sensor color electronic camera," U.S. Patent 5 629 734, May, 1997.

[6] R. Kimmel, "Demosaicing: Image reconstruction from ccd samples," *IEEE Trans. Image Proc.*, vol. 8, no. 9, pp. 1221–1228, Sept. 1999.

[7] X. Wu and N. Zhang, "Primary-consistent soft-decision color demosaicking for digital cameras," *IEEE Trans. Image Proc.*, vol. 13, no. 9, pp. 1263–1274, Sept. 2004.

[8] K. Hirakawa and T. W. Parks, "Adaptive homogeneity-directed demosaicing algorithm," *IEEE Trans. Image Proc.*, vol. 14, no. 3, pp. 360–369, Mar. 2005.

[9] D. Menon, S. Andriani, and G. Calvagno, "Demosaicing with directional filtering and *a posteriori* decision," *IEEE Trans. Image Proc.*, vol. 16, no. 1, pp. 132–141, Jan. 2007.

[10] N. Zhang and X. Wu, "Color demosaicking via directional linear minimum mean square-error estimation," *IEEE Trans. Image Proc.*, vol. 14, no. 12, pp. 2167–2177, Dec. 2005.

[11] D. Alleysson, S. Süsstrunk, and J. Hérault, "Linear demosaicing inspired by the human visual system," *IEEE Trans. Image Proc.*, vol. 14, no. 4, pp. 439–449, Apr. 2005.

[12] N. Lian, L. Chang, and Y.-P. Tan, "Improved color filter array demosaicking by accurate luminance estimation," in *IEEE Proc. Int. Conf. Image Proc.*, vol. 1, Sept. 2005, pp. 41–44.

[13] S. Mallat and S. Zhong, "Characterization of signals from multiscale edges," *IEEE Trans. Pattern Anal. Machine Intell.*, vol. 14, no. 7, pp. 710–732, Jan. 1992.

[14] S. G. Chang, Z. Cvetković, and M. Vetterli, "Locally adaptive wavelet-based image interpolation," *IEEE Trans. Image Proc.*, vol. 15, no. 6, pp. 1471–1485, June 2006.